HHS Public Access

Author manuscript

*Cell*. Author manuscript; available in PMC 2018 April 06.

Published in final edited form as:

*Cell*. 2017 April 06; 169(2): 301–313.e11. doi:10.1016/j.cell.2017.03.011.

# RIPK3 restricts viral pathogenesis via cell death-independent neuroinflammation

**Brian P. Daniels**[1], **Annelise G. Snyder**[1], **Tayla M. Olsen**[1], **Susana Orozco**[2], **Thomas H. Oguin III**[3], **Stephen W.G. Tait**[4], **Jennifer Martinez**[3], **Michael Gale Jr.**[1,5], **Yueh-Ming Loo**[1,5,*], and **Andrew Oberst**[1,5,6,*]

[1]Department of Immunology, University of Washington, Seattle, WA 98109, USA

[2]Molecular and Cellular Biology Program, University of Washington, Seattle, WA 98109, USA

[3]Immunity, Inflammation, and Disease Laboratory, NIEHS, National Institutes of Health, Research Triangle Park, NC 27709, USA

[4]Cancer Research UK Beatson Institute, Institute of Cancer Sciences, University of Glasgow, Glasgow G61 1BD, UK

[5]Center for Innate Immunity and Immune Disease, University of Washington, Seattle, WA 98109 USA

## Summary

Receptor-interacting kinase-3 (RIPK3) is an activator of necroptotic cell death, but recent work has implicated additional roles for RIPK3 in inflammatory signaling independent of cell death. However, while necroptosis has been shown to contribute to antiviral immunity, death-independent roles for RIPK3 in host defense have not been demonstrated. Using a mouse model of West Nile virus (WNV) encephalitis, we show that RIPK3 restricts WNV pathogenesis independently of cell death. *Ripk3*$^{-/-}$ mice exhibited enhanced mortality compared to WT controls, while mice lacking the necroptotic effector MLKL, or both MLKL and caspase-8, were unaffected. The enhanced susceptibility of *Ripk3*$^{-/-}$ mice arose from suppressed neuronal chemokine expression and decreased central nervous system (CNS) recruitment of T lymphocytes and inflammatory myeloid cells, while peripheral immunity remained intact. These data identify pleiotropic functions for RIPK3 in the restriction of viral pathogenesis, and implicate RIPK3 as a key coordinator of immune responses within the CNS.

Correspondence: looy@uw.edu (YML), oberst@uw.edu (AO).
[6]Lead Contact

**Author Contributions**

Conceptualization: BPD, MG, YML, AO. Methodology: BPD, YML, and AO. Analysis: BPD, AGS, THO, SO, YML. Investigation: BPD, AGS, TMO, SO, TH, YML. Resources: SWT, JM, MG. Writing- Original Draft: BPD. Writing- Review and Editing: BPD, AGS, TMO, YML, AO. Supervision and Funding Acquisition: JM, MG, YML, AO.

## Introduction

Necroptosis is a form of programed cell death coordinated by receptor-interacting kinases 1 (RIPK1) and 3 (RIPK3). Stimuli including death receptor and pattern recognition receptor (PRR) ligation induce the activation of RIPK3 and the downstream phosphorylation of mixed lineage kinase domain-like protein (MLKL). MLKL serves as an executioner protein, promoting cell death via plasma membrane disruption and cell rupture (Cho et al., 2009; Wang et al., 2014a). While the molecular mechanisms that orchestrate necroptosis have been the subject of intense investigation, the physiological relevance of necroptosis during infection and injury are less well defined (Oberst, 2015). Moreover, recent studies have suggested surprising roles for RIPK1 and RIPK3 in promoting inflammation independently of cell death signaling, indicating that these proteins may serve pleiotropic and context-dependent functions in host immune responses (Lawlor et al., 2015; Moriwaki and Chan, 2016; Najjar et al., 2016; Newton et al., 2016).

RIPK3 signaling has been implicated in the control of diverse viral infections, including influenza A virus (IAV) (Nogusa et al., 2016), *Vaccinia* virus (Cho et al., 2009; Pan et al., 2014) herpes simplex virus-1 (HSV-1) (Huang et al., 2015), and murine cytomegalovirus (MCMV) (Upton et al., 2010, 2012). However, evidence of death-independent, RIPK3-mediated control of viral infections remains limited. Of note, the involvement of RIPK3 in the restriction of neuroinvasive infections is not known, and studies of the role of RIPK3 in defense against potentially neuroinvasive viruses such as HSV and CMV have thus far been limited to models of peripheral infection.

West Nile virus (WNV) is an encephalitic flavivirus of global concern. WNV cycles in nature between avian and mosquito reservoirs, with incidental infection of mammals, including humans. After peripheral infection, WNV replicates in lymphoid tissues before entering the central nervous system (CNS) in a subset of human hosts. Neuroinvasive WNV infection is fatal in many patients, while survivors are often left with severe cognitive and neurologic sequelae (Sejvar et al., 2003; Vasek et al., 2016). Neuroimmune control of WNV infection requires robust innate immune responses among resident CNS cells, as well as recruitment of infiltrating peripheral leukocytes (Cho and Diamond, 2012; Daniels and Klein, 2015; Suthar et al., 2013). However, CNS immune responses must be carefully regulated, as neural tissue is susceptible to immunologic injury and is limited in its capacity for repair (Daniels et al., 2017; Wang et al., 2003). Thus, uncovering the mechanisms that promote protective versus pathologic CNS inflammation during neurotropic flavivirus infection is critical for the development of targeted treatments, none of which currently exist (Kok, 2016).

Here, we demonstrate a previously unknown function for RIPK3 in the coordination of protective neuroinflammation during WNV infection that is independent of MLKL-driven necroptosis. Using a mouse model of WNV encephalitis, we show that mice lacking RIPK3 or the kinase activity of RIPK1, but not those lacking MLKL or both MLKL and Caspase-8, exhibit enhanced susceptibility to fatal WNV infection. While RIPK3 was dispensable for clearing WNV infection in peripheral compartments, *Ripk3*$^{-/-}$ mice failed to effectively restrict infection within the CNS due to decreased recruitment of infiltrating leukocytes. Our

studies demonstrate that RIPK3 promotes neuroinflammation during WNV infection by driving the neuronal expression of inflammatory chemokines in a manner that requires its kinase activity and that of RIPK1. These findings uncover a critical physiologic function for death-independent, RIPK3-driven inflammation in restricting a neurotropic viral infection of significant public health concern.

## Results

### RIPK3 restricts WNV infection independent of induction of cell death

To assess the role of RIPK3 and MLKL in controlling WNV pathogenesis, we infected *Ripk3*$^{-/-}$, *Mlkl*$^{-/-}$, and age/sex matched controls subcutaneously via footpad with 100pfu of the virulent WNV-TX 2002-HC strain, then monitored mice for survival and the development of clinical signs of disease. We found *Ripk3*$^{-/-}$ mice to be highly susceptible to WNV infection, exhibiting accelerated and uniform mortality compared to congenic C57BL/6/NJ (B6/N) controls (Figure 1A). Increased mortality in *Ripk3*$^{-/-}$ mice was accompanied by earlier and more severe development of clinical signs of disease burden (Figure 1B). In contrast, survival and disease burden in mice lacking the necroptotic effector MLKL (*Mlkl*$^{-/-}$) were indistinguishable from congenic C57BL/6J (B6/J) controls (Figure 1C, Figure S1A). A recent study of IAV pathogenesis found that upon loss of MLKL, RIPK3 signaling could alternatively mediate host defense through engagement of caspase-8 mediated apoptosis (Nogusa et al., 2016). In contrast, we found that mice lacking both MLKL and caspase-8 (*Mlkl*$^{-/-}$*Casp8*$^{-/-}$) responded similarly to littermate *Mlkl*$^{-/-}$ *Casp8*$^{+/+}$ controls upon WNV infection (Figure S1B–C). These data suggested a critical role for RIPK3 in the restriction of WNV infection that was, surprisingly, independent of MLKL-dependent programmed necrosis or caspase-8-dependent apoptosis.

We next assessed whether WNV was capable of inducing RIPK3-dependent cell death in myeloid or neuronal cells, two host cell types permissive to WNV infection, by monitoring cell death via an IncuCyte imaging platform (Orozco et al., 2014). Infection of bone marrow-derived macrophages (BMDMs) with WNV (MOI 0.01) resulted in minimal cell death in both B6/N and *Ripk3*$^{-/-}$ BMDMs that was indistinguishable from death observed in mock-infected controls. However, WNV induced substantial cell death in the presence of the pan-caspase inhibitor zVAD in B6/N, but not *Ripk3*$^{-/-}$, BMDMs (Figure 1D), suggesting that WNV can induce RIPK3-dependent necroptosis only under conditions of caspase inhibition. In contrast, infection of primary cerebral cortical neuron cultures (MOI 0.001) resulted in modest cell death (Figure 1D). However, this cell death was RIPK3-independent, as WNV-induced cell death was similar in both B6/N and *Ripk3*$^{-/-}$ cultures. Instead, WNV-induced neuronal cell death was dependent on caspase activity, as it was completely blocked in cultures of both genotypes by zVAD treatment, consistent with prior reports demonstrating WNV-induced neuronal apoptosis (Michaelis et al., 2007; Samuel et al., 2007). Histopathologic analysis of CNS tissue sections from WT or *Ripk3*$^{-/-}$ mice 9 days post infection (dpi) revealed no evidence for necrotic cell death in the CNS of mice of either genotype (Figure S1D). Together, these data indicate that, in key myeloid and CNS cell types targeted by WNV, infection alone does not trigger RIPK3-dependent cell death. Notably, while BMDMs could be induced to undergo RIPK3-dependent cell death in

response to WNV infection combined with caspase inhibition, neurons were resistant to RIPK3-dependent death in these conditions.

To further investigate the function of RIPK3 in controlling WNV infection, we measured viral burden in key target tissues following subcutaneous inoculation. These studies revealed transiently higher viral burden in *Ripk3*$^{-/-}$ mice in some peripheral compartments, including serum (Figure 1E) and spleen (Figure 1F), while viral burden was unchanged in draining inguinal lymph nodes (Figure 1G) and kidney (Figure 1H). Despite higher splenic and serum viral loads early after infection, *Ripk3*$^{-/-}$ mice were nevertheless able to control infection in these compartments, with viral titers returning to levels observed in B6/N controls by 8 dpi. Peripheral immunity to WNV remained intact in *Ripk3*$^{-/-}$ mice, which were similar to B6/N controls when comparing overall numbers and relative frequencies of all T cell and myeloid subsets analyzed in spleens on 8 dpi (Figure S2A–C). Moreover, numbers of antigen-specific T cells identified by staining with a tetramer displaying the immunodominant WNV peptide $D^b$-NS4B were similar between genotypes (Figure S2B). Overall numbers of splenic B cells and serum WNV-neutralizing antibody titers were also similar in *Ripk3*$^{-/-}$ mice compared to WT controls (Figure S2D). Together, these data indicate that the increased pathogenesis observed in *Ripk3*$^{-/-}$ mice after WNV infection was not due to impaired peripheral cellular immunity or a failure to control infection in peripheral compartments.

## RIPK3 is required for control of WNV burden within the CNS

In contrast to our observations in peripheral tissues, we observed significantly increased viral loads in *Ripk3*$^{-/-}$ mice across multiple CNS tissues, including cerebral cortex (Figure 2A), brainstem (Figure 2B), cerebellum (Figure 2C), and spinal cord (Figure 2D). Unlike peripheral viral loads, increased CNS viral burden did not resolve to WT levels in *Ripk3*$^{-/-}$ mice by 8 dpi. Similar to our survival studies, RIPK3-dependent control of tissue viral burden was MLKL-independent, as WNV titers were indistinguishable in *Mlkl*$^{-/-}$ mice compared to WT controls in all compartments analyzed (Figure S3A–B). Combined with our observation that peripheral immunity appears intact in *Ripk3*$^{-/-}$ mice, this finding indicates that RIPK3 may play a CNS-intrinsic role in the control of neuroinvasive WNV infection.

To test whether the protective function of RIPK3 was intrinsic to the CNS, we performed intracranial inoculation experiments, which allow examination of CNS viral replication kinetics and immune responses without possible confounding factors arising from differential neuroinvasion. While intracranial WNV infection results in 100% mortality in mice, *Ripk3*$^{-/-}$ mice exhibited an acceleration of this mortality compared to WT controls (Figure 2E). Analysis of viral burden in whole brains following intracranial inoculation revealed that WNV titers were similar between genotypes early after infection (2 dpi) (Figure 2F), while titers were increased in *Ripk3*$^{-/-}$ mice compared to controls at later time points (4 and 6 dpi), suggesting that enhanced viral burden and accelerated mortality in *Ripk3*$^{-/-}$ mice were not due to early innate control of viral replication. To reinforce this conclusion, and to test whether there might be a cell-intrinsic function of RIPK3 in controlling viral replication in target CNS cells, we performed multistep growth curve analysis of WNV replication in cultured cerebral cortical neurons and cerebellar granule cell

(GC) neurons (Figure 2G). We observed no detectable difference in viral replication in *Ripk3*$^{-/-}$ neurons of either type. Together, these findings indicate that RIPK3 is required to control WNV infection within the CNS, but that its role is not to limit viral replication within neurons.

## RIPK3 is required for normal chemokine production in neurons

We next questioned whether, in lieu of suppressing viral replication, RIPK3 regulated the expression of key inflammatory mediators in neurons during WNV infection. Examination of cytokine and chemokine protein levels in supernatants of *in vitro* B6/N and *Ripk3*$^{-/-}$ cortical neuron cultures infected with WNV revealed no difference in the expression of the inflammatory cytokines TNF-α and IL-1β (Figure S4A). In contrast, *Ripk3*$^{-/-}$ neuronal cultures exhibited decreased expression of several chemokines, including CCL2, CCL5, CCL11, CXCL1, CXCL9, and CXCL10 (Figure 3A; Figure S4B) following WNV infection. As CCL2 and CXCL10 are both important regulators of neuroinflammation during WNV infection (Klein et al., 2005; Lim et al., 2011), we focused subsequent investigations on these two chemokines. Subsequent qRT-PCR experiments in WNV-infected cortical neuron cultures revealed that decreased chemokine expression in *Ripk3*$^{-/-}$ cultures was apparent at the mRNA level (Figure 3B), suggesting that RIPK3 promotes the transcription of inflammatory chemokines during neuronal WNV infection.

Activation of RIPK3 can occur downstream of diverse toll-like receptors (TLRs), via both TRIF and Myd88-dependent pathways (He et al., 2011; Kaiser et al., 2013). To assess whether RIPK3-driven neuronal chemokine expression was unique to WNV infection or if it could be triggered by other inflammatory stimuli, we treated primary cortical neuron cultures with the synthetic double-stranded RNA analog poly(I:C), a stimulus that activates TLR3 in neurons (Cameron et al., 2007). These experiments revealed decreased CCL2 and CXCL10 protein (Figure 3C) and mRNA (Figure 3D) expression in *Ripk3*$^{-/-}$ cultures compared to B6/N controls, suggesting that direct PRR stimulation was sufficient to induce RIPK3-dependent chemokine expression in the absence of active infection. Notably, we did not observe significant differences in poly(I:C)-induced expression of the inflammatory cytokines TNFα and IL-1β in *Ripk3*$^{-/-}$ neurons compared to B6/N controls (Figure S4C), consistent with our findings in WNV-infected neurons. Furthermore, we did not observe evidence for RIPK3-dependent cytokine or chemokine expression in either BMDMs or cultured microglia following treatment with TLR ligands (Figure S4D–E). Together, these findings imply that RIPK3 may have a specific role in the coordination of PRR-induced chemokine expression in neuronal lineage cells of the CNS.

To gain a more general understanding of the role of RIPK3 in coordinating neuronal chemokine expression, we assessed whether the kinase activity of RIPK3, or of its interactor RIPK1, was involved in chemokine expression downstream of additional TLR agonists, using the TLR3 agonist poly(I:C) (Figure 3E), the TLR4 agonist LPS (Figure 3F), and the TLR7 agonist CL264 (Figure 3G). To determine if the kinase activity of the RIP kinases was involved, we additionally treated neurons with the RIPK3 inhibitor GSK 843 (Mandal et al., 2014) or the RIPK1 inhibitor Necrostatin-1 (Nec) (Degterev et al., 2008). We found that pharmacological blockade of either RIPK1 or RIPK3 resulted in suppressed CCL2 protein

expression in WT neuronal cultures to levels similar to *Ripk3*$^{-/-}$ cultures, suggesting that RIPK3-dependent chemokine expression downstream of multiple TLRs requires the kinase activity of both RIPK1 and RIPK3. Neither inhibitor impacted CCL2 expression in *Ripk3*$^{-/-}$ cultures, indicating that the effects of these inhibitors in WT cultures were specific to blockade of signaling through RIPK3. In contrast, CCL2 expression following treatment with the pan-caspase inhibitor QVD was not affected in either genotype, suggesting that caspase signaling is not involved in RIPK3-driven neuronal chemokine expression. Though Necrostatin-1 has been widely used to inhibit RIPK1 kinase activity, off-target effects have been reported (Takahashi et al., 2012). We therefore repeated our Necrostatin-1 experiments using the more specific RIPK1 inhibitor GSK 963 (Berger et al., 2015) and observed very similar results (Figure S4F). To further establish a requirement for RIPK1 kinase activity in RIPK3-mediated neuronal chemokine expression, we generated neuronal cultures from RIPK1 kinase-dead knock-in (*Ripk1*$^{KD/KD}$) mice (Berger et al., 2014), in which an inactivating point mutation has been introduced into the catalytic domain of RIPK1. *Ripk1*$^{KD/KD}$ neuronal cultures exhibited decreased expression of CCL2 and CXCL10 after either WNV infection (Figure 3H) or poly(I:C) treatment (Figure 3I). Consistent with a role for the kinase activity of RIPK1 in a protective chemokine response during WNV infection, *Ripk1*$^{KD/KD}$ mice exhibited accelerated and uniform mortality (Figure 3J) and more severe clinical symptoms (Figure S4G) compared to B6/J controls, similar to those observed in *Ripk3*$^{-/-}$ mice, after subcutaneous infection with WNV.

We next sought to confirm a role for RIPK3 in chemokine expression following TLR stimulation or WNV infection in neural cells of human origin. To do this, we tested the effect of poly(I:C) or WNV on three separate human neuroblastoma cell lines (Teitz et al., 2000) differentiated into neuron-like cells by culture in retinoic acid and brain-derived neurotropic factor (BDNF) (Encinas et al., 2000). Upon poly(I:C) treatment or WNV infection, all three of these cell lines produced CCL2. This response was significantly reduced in all three cell lines by co-treatment with GSK 872, an inhibitor of human RIPK3 (Mandal et al., 2014) (Figure S5A). Analogous to the results obtained with *Ripk3*$^{-/-}$ murine neurons, inhibition of RIPK3 did not cause cell-intrinsic differences in viral growth kinetics in human neuroblastoma cells, nor did it affect cell death following WNV infection (Figure S5B–C). Together, these studies indicate that the kinase activity of RIPK1 and RIPK3 is engaged by both TRIF and Myd88-dependent TLR signaling in neurons, that this activity drives robust neuronal chemokine expression, and that the kinase activity of RIPK1 is required for protective immunity to WNV infection.

## Activation of RIPK3 in neurons triggers chemokine production, not cell death

We next assessed whether direct activation of RIPK3 in the absence of any exogenous immune stimulus was sufficient to drive neuronal chemokine expression. To do this, we created mice expressing a chimeric RIPK3 protein fused to two copies of FKBP$^{F36V}$ (RIPK3-2xFV). The FKBP domains of this fusion protein bind with high affinity to a synthetic homologue of rapamycin referred to here as “AP1.” AP1 treatment induces a rapid, FKBP-mediated oligomerization of RIPK3-2xFV proteins, leading to the activation of RIPK3 and recruitment of RIPK1 in the absence of any endogenous upstream signal (Orozco et al., 2014). For these studies, we generated mice expressing the RIPK3-2xFV

construct preceded by a *lox-stop-lox* element and followed by a T2A-mCherry sequence, driven by the *Rosa26* promoter (Figure 4A). These mice were crossed to mice expressing Cre recombinase under the ubiquitously expressed *Meox2* (Mox2) promoter, resulting in Cre-mediated excision of the inserted stop codon (Figure 4B). Transgene expression was confirmed in primary murine embryonic fibroblasts (MEFs) via western blot for FKBP (Figure 4C) and fluorescent immunocytochemical detection of mCherry (Figure 4D). Similar to our previous studies using a related construct in NIH-3T3 cells (Orozco et al., 2014; Yatim et al., 2015), AP1 treatment of RIPK3-2xFV expressing primary MEFs resulted in robust cell death and chemokine expression in Mox2-Cre$^+$ cultures (Figure 4E–F), but did not impact cell viability or chemokine expression in Mox2-Cre$^-$ cultures. Further experiments confirmed both FKBP and mCherry expression in primary cortical neurons cultured from RIPK3-2xFV$^+$ Mox2-Cre$^+$ mice (Figures 4C and 4G). Strikingly, AP1 treatment of RIPK3-2xFV$^+$ Mox2-Cre$^+$ neurons did not induce cell death (Figure 4H). However, AP1 treatment did potently induce chemokine expression in RIPK3-2xFV$^+$ Mox2-Cre$^+$ neurons in a manner that required the kinase activity of RIPK3, as the RIPK3 inhibitor GSK 843 blocked AP1-mediated neuronal chemokine expression (Figure 4I). We previously demonstrated that RIPK3 oligomerization triggers the recruitment and activation of RIPK1. Consistent with these findings, and with a role for the kinase activity of RIPK1 in the observed chemokine production, we found that co-treatment with the RIPK1 inhibitor Nec1 also abrogated AP1-induced chemokine expression in RIPK3-2xFV$^+$ Mox2-Cre$^+$ neurons. These data indicate that direct activation of RIPK3 alone is sufficient to induce death-independent chemokine expression in neurons.

## RIPK3 is required for normal chemokine production in the CNS upon WNV infection

To confirm that RIPK3 contributed to CNS chemokine expression *in vivo*, we analyzed brain homogenates from WT and *Ripk3*$^{-/-}$ mice following either subcutaneous or intracranial WNV infection. Consistent with our *in vitro* results using neuronal cultures, brains of *Ripk3*$^{-/-}$ mice exhibited decreased CCL2 and CXCL10 expression compared to B6/N controls following both subcutaneous (Figure 5A) and intracranial (Figure 5B) infection. Additional experiments revealed that CCL2 and CXCL10 mRNA levels were similarly decreased in *Ripk3*$^{-/-}$ brains in both infection models (Figure 5C–D). Brains of WNV-infected *Ripk3*$^{-/-}$ mice exhibited decreased expression of additional chemokines, including CCL11, CXCL1, and CXCL9, though the impact of RIPK3 on expression of these additional chemokines was variable between infection routes (Figure S6A–B). In contrast, brains of *Mlkl*$^{-/-}$ mice exhibited levels of chemokine expression after subcutaneous WNV infection that were indistinguishable from B6/J controls (Figure S6C).

## RIPK3 coordinates immune cell infiltration into the CNS upon WNV infection

As mice lacking RIPK3 exhibited diminished expression of leukocyte chemoattractants in the CNS during WNV infection, we questioned whether this would result in poor CNS recruitment of inflammatory cells. Flow cytometric analysis of leukocytes isolated from whole brains at 8 dpi following subcutaneous inoculation revealed significantly decreased recruitment of multiple subsets of infiltrating cells in the CNS of *Ripk3*$^{-/-}$ mice, including CD4$^+$ and CD8$^+$ T cells (Figure 6A–B). Notably, *Ripk3*$^{-/-}$ mice were also impaired in their ability to recruit antigen-specific CD8$^+$ T cells to the CNS, exhibiting both decreased

relative percentages and overall numbers of WNV-NS4B tetramer$^+$ CD8$^+$ cells (Figure 6C–D). Analysis of infiltrating myeloid cell populations also revealed decreased frequencies of infiltrating CD45$^{hi}$ cells among total CD11b$^+$ cells (Figure 6E–F). While *Ripk3*$^{-/-}$ mice exhibited decreased numbers of infiltrating CD45$^{hi}$ CD11b$^+$ F4/80$^+$ monocytes/macrophages and CD45$^{hi}$ CD11c$^+$ MHCII$^+$ antigen presenting cells, overall numbers of CD45$^{lo}$ CD11b$^+$ F4/80$^+$ resident microglia were unaltered, suggesting that decreased myeloid cell numbers in the *Ripk3*$^{-/-}$ CNS are due to impaired recruitment of infiltrating cells and not defects in resident immune cell populations. Critically, neither *Mlkl*$^{-/-}$ nor *Mlkl*$^{-/-}$*Casp8*$^{-/-}$ mice exhibited defects in CNS recruitment of any immune cell subset after WNV infection (Figure S7A–B), suggesting that programmed cell death does not contribute to RIPK3-mediated neuroinflammation. Together, these data indicate that RIPK3 is required to coordinate the recruitment of a wide variety of immune cell subsets into the CNS following neuroinvasive WNV infection, and that it does so in a cell death-independent manner.

### RIPK3 contributes to CNS recruitment of CCR2$^+$ and CXCR3$^+$ infiltrating leukocytes

To assess whether decreased CCL2 and CXCL10 expression specifically contributed to decreased neuroinflammation in WNV-infected *Ripk3*$^{-/-}$ mice, we performed additional flow cytometric analysis using markers for the CCL2 receptor, CCR2, and the CXCL10 receptor, CXCR3. In brain tissues analyzed on day 8 after subcutaneous infection, *Ripk3*$^{-/-}$ mice exhibited decreased percentages of CXCR3$^+$ cells among CD3$^{hi}$ T lymphocytes, as well as decreased percentages of CCR2$^+$ cells among CD11b$^+$ myeloid cells compared to WT controls (Figure 7A–B). Decreased recruitment of CXCR3$^+$ lymphocytes extended to both CD4$^+$ and CD8$^+$ T cell subsets (Figure 7C). We also observed decreased numbers of CD45$^{hi}$ CD11b$^+$ F4/80$^+$ CCR2$^+$ inflammatory monocytes (Figure 7D). Whole brain homogenates also exhibited decreased mRNA expression of both CXCR3 and CCR2 (Figure 7E). While some of this chemokine receptor expression is derived from resident CNS cells, these data support the notion of decreased CXCR3 and CCR2 expressing infiltrating cells in the brains of *Ripk3*$^{-/-}$ mice. Ultimately, these findings suggest that RIPK3-dependent expression of CXCL10 and CCL2 is necessary for robust recruitment of antiviral leukocytes to the CNS during WNV infection.

## Discussion

Despite their profound and growing burden to global public health, the factors that govern pathogenesis and host control of neurotropic infections remain incompletely understood. Here, we demonstrate a previously unknown function for RIPK3 in coordinating protective neuroinflammation during neuroinvasive West Nile virus infection. Remarkably, RIPK3 restricted WNV pathogenesis in a necroptosis-independent manner, as WNV did not induce necroptosis in primary neuronal cultures and both MLKL and caspase-8 were dispensable for the protective effects of RIPK3 *in vivo*. While RIPK3 did not directly influence viral replication within neurons, it was necessary for robust neuronal chemokine expression and the CNS recruitment of infiltrating antiviral leukocytes, an effect that also required the kinase activity of RIPK1. These findings identify RIPK3 as a key neuronal regulator of CNS inflammation during flavivirus encephalitis.

*In vivo* neuronal expression of RIPK3 has been established by several recent reports and appears to contribute to inflammation and pathogenesis in rodent models of cerebral ischemia/reperfusion injury (Xu et al., 2016), lysosomal storage disorders (Vitner et al., 2014), and traumatic brain injury (Liu et al., 2016). RIPK3 is also expressed in glia, including microglia, astrocytes, and oligodendrocytes, where it has been shown to contribute to the pathogenesis of rodent and human neurodegeneration, CNS autoimmunity, and demyelination (Ito et al., 2016; Ofengeim et al., 2015; Re et al., 2014). While the potential for RIPK3 to induce neuroinflammatory pathogenesis has been well established by these prior reports, our study instead demonstrates an indispensable, protective role for RIPK3-mediated neuroinflammation and establishes RIPK3 as a critical host factor in controlling neurotropic viral infection. Our study focused on RIPK3-dependent effects in neurons, as they are the primary CNS target of WNV and exhibit robust chemokine expression during infection (Getts et al., 2008; Klein et al., 2005). While we did not observe a requirement for RIPK3 signaling in chemokine production by microglia, our results cannot rule out additional roles for this pathway in non-neuronal cells of the CNS. We also note efforts that are currently underway to develop RIPK1 inhibitors with activity in the CNS as a treatment for neurodegeneration and ischemic injury. Our findings indicate that such compounds may also increase susceptibility to neuroinvasive viral infection.

A key finding in our study is the contribution of RIPK3 to the chemotactic milieu that supports protective antiviral neuroinflammation. Neuronal expression of chemokines has been well established to underlie successful antiviral immunity during WNV infection, contributing to leukocyte influx and viral clearance (Bardina et al., 2015; Durrant et al., 2015; Klein et al., 2005). Beyond the context of infection, CNS chemokines also serve critical roles in CNS homeostasis, development, neurotransmission, and repair (Durrant et al., 2014b; Ransohoff and Trettel, 2015; Reaux-Le Goazigo et al., 2013; Williams et al., 2014a). Our findings raise the additional possibility that RIPK3 may serve previously unknown chemokine-mediated functions in a diverse array of neurologic processes.

Our study and other reports (Lawlor et al., 2015; Moriwaki and Chan, 2016; Najjar et al., 2016; Newton et al., 2016; Wang et al., 2014b) demonstrate a capacity for RIPK3 to induce inflammation independently of necroptosis. While recent studies have demonstrated a death-independent role for RIPK3 in NLRP3 inflammasome activation (Lawlor et al., 2015; Wang et al., 2014b) as well as noncanonical IL-1β processing in myeloid cells (Moriwaki et al., 2015), our study did not uncover any impact on IL-1β mRNA or protein expression in *Ripk3*$^{-/-}$ neuronal cultures or brain tissues following WNV infection. Moreover, the phenotype of *Ripk3*$^{-/-}$ mice following WNV infection is markedly different than mice lacking the IL-1 receptor or the inflammasome adaptor ASC, which both exhibit elevated CNS chemokine expression and enhanced, but not protective, neuroinflammation (Durrant et al., 2014a; Durrant et al., 2013; Kumar et al., 2013; Ramos et al., 2012). Thus, death-independent functions for RIPK3 may differ significantly by inflammatory stimulus and host cell type.

Consistent with this idea, we found that in neurons, but not in bone marrow-derived myeloid cells or microglia, chemokine expression stimulated by TLR agonists or WNV infection required the kinase activity of both RIPK1 and RIPK3. Also consistent with this finding,

mice expressing a kinase-dead form of RIPK1 displayed increased susceptibility to WNV infection similar to that observed in *Ripk3*$^{-/-}$ mice. We also found that even direct activation of RIPK3 in neurons failed to trigger necroptosis, but rather promoted chemokine expression. Further molecular mechanisms that govern the functions of RIPK1 and RIPK3 in these contexts remain the subject of ongoing investigation, though our study provides some initial insights. For example, in contrast with recent reports using cultured myeloid cells (Ito et al., 2016), in neurons we observed that the requirement for RIPK1 and RIPK3 kinase activity downstream of TLR ligation did not require inhibition of the caspases. While we report an unexpected requirement for RIPK1 and RIPK3 signaling downstream of TLR ligation in neurons, our findings do not rule out engagement of RIPK signaling by other innate immune pathways during WNV infection of these cells. Together, our findings indicate an unexpected diversity in the outcomes of RIPK1 and RIPK3 signaling between cell types and imply additional obligate functions for this pathway within the CNS that are not observed in other tissues.

## STAR Methods

### CONTACT FOR REAGENT AND RESOURCE SHARING

Further information and requests for resources and reagents should be directed to and will be fulfilled by the lead contact, Andrew Oberst (oberst@uw.edu).

### EXPERIMENTAL MODEL AND SUBJECT DETAILS

**Mice—***Ripk3*$^{-/-}$ (Newton et al., 2004), *Mlkl*$^{-/-}$ (Murphy et al., 2013), *Casp8*$^{-/-}$ (Beisner et al., 2005), *Mlkl*$^{-/-}$ *Casp8*$^{-/-}$, *RIPK1*$^{KD/KD}$ (Berger et al., 2014), and RIPK3-2xFV$^{fl/fl}$ Mox2-Cre$^{+}$ mice in this study were bred and housed under specific-pathogen free conditions at the University of Washington. Wild-type C57BL/6NJ and C57BL/6J controls were either obtained commercially (Jackson Laboratories) or bred in-house. *Ripk3*$^{-/-}$ animals were congenic to the C57BL/6NJ background, while all other strains were on the C57BL/6J background; in all cases wild-type controls of appropriate sub-strain were used. Mox2-Cre$^{+}$ mice were obtained commercially (Jackson Laboratories, strain 003755) and maintained at hemizygosity. RIPK3-2xFV$^{fl/-}$ mice were produced for the authors by inGenious Targeting Laboratory (Rankonkoma, NY).

RIPK3-2xFV$^{fl/fl}$ mice were generated using a vector containing a FLAG tag, followed by a chimeric version of RIPK3 fused to two copies of FKBP$^{F36V}$ (RIPK3-2xFV), followed by a T2A-mCherry sequence (Figure S5A). This entire sequence was cloned into the MluI site of a ROSA26-stop backbone vector using conventional cloning methods. The stop cassette in the ROSA-stop backbone vector contains a splice acceptor and a stop cassette flanked by lox-p sites and is inserted in intron 1 of the *Rosa*26 locus. The FLAG-RIPK3-T2A-mCherry sequence is inserted immediately downstream of the stop cassette.

Genotyping of the RIPK3-2xFV transgene and confirmation of a deleted stop cassette was accomplished using multiple PCR reactions (Figure 4B). Two separate reactions were used to detect the presence of the RIPK3-2xFV transgene (349bp product) and the transgene with a deleted stop cassette (603bp product). Homozygosity of the transgene was assessed by

confirming the absence of a WT Rosa26 locus (346bp product). Mox2-Cre expression was confirmed by the presence of a mutant (300bp) product as compared to a WT (410bp) product. See Table S1 for primer sequences. PCR reactions were performed with EconoTaq reagents (Lucigen) using genomic DNA extracted from ear tissue according to standard protocols.

**Cell culture and infections—**Primary macrophage cultures were generated from bone marrow via differentiation in 40 ng/ml M-CSF, as described (Samuel et al., 2006). Embryonic fibroblasts were generated and maintained as previously described (Szretter et al., 2012). Primary cultures of cerebral cortical neurons and purified cerebellar granule cell neurons were generated using E15 embryos or P3 neonatal mice, as described (Klein et al., 2005). Purified microglia were obtained from mixed glial cultures generated from P1-P3 neonatal mice as described (Williams et al., 2014b). Human neuroblastoma cell lines NB8, NB15, NB16 were maintained in a 1:1 mixture of DMEM and Ham's F-12 Nutrient Mix (ThermoFisher). Neuroblastoma cells were differentiated into neuron-like cells by supplementing culture medium with 10μM *all-trans* retinoic acid (Sigma-Aldrich) and 50ng/ml recombinant human BDNF (Peprotech), as described (Encinas et al., 2000). For infection experiments, macrophage and cultures were infected at MOI 0.01, while primary neuronal cultures and neuroblastoma cell lines were infected at MOI 0.001.

**Virus and virologic assays—**WNV strain TX 2002-HC (WNV-TX) was plaque purified as described (Keller et al., 2006) and passaged twice through mycoplasma-free Vero cells. Viral stock titers, as well as titers from experimental tissues and culture supernatants, were determined by plaque assay on BHK21-15 cells or qRT-PCR using WNV positive strand-specific primers (Brien et al., 2013). Anti-WNV neutralizing antibodies in serum were measured using a plaque reduction neutralization assay as previously described (Diamond et al., 2003).

## METHOD DETAILS

**Mouse infections—**Subcutaneous WNV infection was performed by injection of 100 pfu WNV-TX in 50 μl of HBSS into a rear footpad. For intracranial infection, 10 pfu WNV-TX was injected in 10 μl of HBSS into the third cerebral ventricle with a guided 29G needle. Infected mice were monitored daily for weight loss and presentation of clinical signs of disease, including hunched posture, ruffled fur, hindlimb weakness, and paresis. Severity of paresis was defined as follows: mild – partial loss of motor function in one hind limb; moderate – complete or nearly complete loss of motor function in one hind limb or partial loss of motor function in both hind limbs; severe – complete or nearly complete loss of motor function in both hind limbs and/or pronounced ataxia. Mice reaching a moribund state or losing more than 20% of initial body weight were euthanized. All experiments were performed in both male and female 8 week old mice, in accordance with protocols approved by the University of Washington Animal Care and Use Committee (IACUC).

**Cell death assays—**Cell death was analyzed using a 2-color IncuCyte Zoom in-incubator imaging system (Essen Biosciences), as previously described (Gutierrez et al., 2017; Orozco et al., 2014). Briefly, dead cells were detected by measuring uptake of the cell impermeable

dye Sytox Green (Life Technologies). Cell death was quantified as a percent of $Sytox^{+}$ cell nuclei out of total cell nuclei (Syto Green+) in culture.

**Tissue preparation and CNS leukocyte isolation—**All tissues harvested from mice for subsequent qRT-PCR, protein, virologic, or flow cytometric analysis were extracted following extensive cardiac perfusion with 30 ml of sterile PBS. Extracted tissues were weighed and homogenized using 1.0 mm diameter zirconia/silica beads (Biospec) in sterile PBS (protein and/or virologic analysis) or RA1 lysis buffer (for RNA isolation, Macherey-Nagel). For histological studies, tissues were fixed, sectioned, and stained as described (Graham et al., 2015). For flow cytometry, leukocytes were isolated from whole brains after digestion in 0.05% collagenase A (Sigma-Aldrich) and 10 μg/ml DNase I (Sigma-Aldrich), then purified via centrifugation in 37% isotonic Percoll (Sigma-Aldrich) as described (Szretter et al., 2012).

**Flow cytometry—**Isolated leukocytes from spleens or brains were stained as described (Durrant et al., 2014a) with fluorescently conjugated antibodies to CD3 (BD, clone 145-2C11), CD4 (BD, clone RM4-5), CD8a (BD, clone 53-6.7), CD11b (BD, clone M1/70), CD11c (BD, clone 565451), CD45.2 (BD, clone 104), CXCR3 (BD, clone CXCR3-173), CCR2 (BD, clone FAB5538A), B220 (BD, clone RA3-682), MHCII (BD, clone M5/114.15.2), F4/80 (BD, clone T45-2342), and $D^{b}$-NS4B tetramer (NIH tetramer core facility). Data collection and analysis were performed using an LSR II Flow Cytometer (BD) and FlowJo software (Treestar).

**RNA isolation and qRT-PCR—**Viral RNA in serum was isolated using a Viral RNA Mini Kit (Qiagen). Total RNA from tissues and cell cultures was isolated using a Nucleospin RNA Kit (Macherey-Nagel). cDNA was synthesized using oligo(dT) random hexamers and SuperScript III Reverse Transcriptase (Life Technologies). Fluorogenic quantitative reverse transcriptase PCR (qRT-PCR) analysis was performed with previously published oligonucleotide primers (Daniels et al., 2017) (Table S1) using Sybr Green reagents and a ViiA 7 Real-Time PCR System (Applied Biosystems). Cycle threshold (CT) values for analyzed cytokine/chemokine genes were normalized to CT values of the housekeeping gene *Gapdh* ($CT_{Target} - CT_{Gapdh} = \Delta CT$) Data were subsequently normalized to baseline control values ($\Delta CT_{experimental} - \Delta CT_{control} = \Delta\Delta CT$. Viral transcript data were normalized against a standard curve of known viral titers to generate pfu-equivalent values (Brien et al., 2013).

**Protein Analysis—**Cytokine and chemokine expression in cell culture supernatants or clarified brain homogenates were measured using a Bio-Plex multiplex mouse cytokine, chemokine, and growth factor multiplex immunoassay and a Bio-Plex 200 (Bio-Rad) instrument according to manufacturer's instructions. CCL2 expression in experiments represented in Figure 7C–E was measured using a CCL2 ELISA Ready-SET-Go kit (eBioscience) and a Synergy™ H1 microplate reader using Gen5™ software (BioTek Instruments, Inc.).

**Western Blot—**Cells were lysed in NP40 lysis buffer (150mM NaCl, 20mM Tris-Cl, 1mM EDTA, 1% NP40 at pH 7.5) containing 1X Halt™ Protease Inhibitor Cocktail (ThermoFisher). Thirty μg of protein were run on a 4–12% Novex™ Tris-Glycine mini gel

(Fisher Scientific) at 100V for 2.5 hours in WB running buffer (24mM tris, 32mM Glycine, 3.5mM SDS) and transferred onto PVDF membrane (ThermoFisher) at 300mAmps for 50 min in transfer buffer (6mM tris, 8mM glycine). Membrane was blocked in 5% reconstituted dry milk in TBS+1% Tween-20 (TBS-T) for 1 hour. Membranes were stained overnight at 4C with primary anti-FKBP (ThermoFisher PA1-026A) and anti-actin (Millipore MAP1501) antibodies in 1% milk in TBS-T. Membranes were then stained with HRP-conjugated secondary antibodies (Santa Cruz sc-2003) for 1h at room temperature. Membranes were developed on film after treating with Pierce ECL Western Blotting Substrate (Pierce).

**Immunocytochemistry—**Fluorescent immunocytochemistry was performed as described (Daniels et al., 2014). Cells were fixed for 10 minutes with 4% paraformaldehyde, permeabilized with 0.1% Triton-X, and blocked with 10% goat serum. Cells were stained using a primary anti-mCherry antibody (Rockland) for 1 hour and goat anti-rabbit AlexaFluor 594 secondary antibody (ThermoFisher) for 15 minutes, both at room temperature. Nuclei were visualized via staining with DAPI (ThermoFisher).

**PRR ligands and chemical agents—**The following PRR ligands and chemical inhibitors were used in cell culture experiments: Poly(I:C) (1 μg/ml, Millipore), LPS-EB Ultrapure (1 μg/ml, Invivogen), CL264 (1 μg/ml, Invivogen), zVAD (50 μM, SM Biochemicals), necrostatin-1 (30 μM, Sigma), GSK 963 (100nM, GlaxoSmithKline), GSK 843 (100nM, GlaxoSmithKline) (Mandal et al., 2014), GSK 872 (100nM, GlaxoSmithKline) and QVD (20 μM, SM Biochemicals), AP1 (100 nM, ClonTech, sold as “BB Homodimerizer”).

## QUANTIFICATION AND STATISTICAL ANALYSIS

Survival experiments were analyzed via log-rank test. WNV titers in mouse tissues were analyzed via nonparametric Mann-Whitney U test. All other experiments were compared with parametric tests, including 2-tailed student’s t-test or 2-way ANOVA, with corrections for repeated measures, where appropriate. A p value $<0.05$ was considered statistically significant for all comparisons. Statistical parameters for individual experiments can be found within the figure legends. All statistical analyses were performed using GraphPad Prism software.

## DATA AND SOFTWARE AVAILABILITY

Raw data are available upon request to the lead contact author. No proprietary software or algorithms were used in this study.

## ADDITIONAL RESOURCES

The following resources were used under material transfer agreement (MTA): *Mlkl*$^{-/-}$ mice (Walter and Elizabeth Hall Institute, Australia), *Casp8*$^{-/-}$ mice (University of California, San Diego), *Ripk3*$^{-/-}$ mice (GlaxoSmithKline), *Ripk1*$^{KD/KD}$ mice (GlaxoSmithKline), GSK inhibitors (GlaxoSmithKline), neuroblastoma cell lines NB8, NB15, and NB16 (St. Jude Children’s Research Hospital).

## Key Resource Table

| REAGENT or RESOURCE | SOURCE | IDENTIFIER |
|---|---|---|
| **Antibodies** | | |
| CD3-PerCP-Cy5.5 | BD Biosciences | Cat# 561108 |
| CD4-BV711 | BD Biosciences | Cat# 563726 |
| CD8-BUV395 | BD Biosciences | Cat# 563786 |
| CD11b-APC-R700 | BD Biosciences | Cat# 564985 |
| CD11c-BV421 | BD Biosciences | Cat# 565451 |
| CD45.2-BUV395 | BD Biosciences | Cat# 565616 |
| CXCR3-BV421 | BD Biosciences | Cat# 562937 |
| CCR2-APC | R&D Systems | Cat# FAB5538A |
| B220-AF700 | BD Biosciences | Cat# 557957 |
| MHCII-PerCP-Cy5.5 | BD Biosciences | Cat# 562363 |
| F4/80-PE | BD Biosciences | Cat# 565410 |
| $D^b$-NS4B tetramer-PE | NIH Tetramer Core | N/A |
| FKBP12 | ThermoFisher | Cat# PA1-026A |
| Actin | Millipore | Cat# MAB1501 |
| Mouse anti-rabbit HRP secondary | Santa Cruz | Cat# Sc-2357 |
| Goat anti-mouse HRP secondary | Santa Cruz | Cat# Sc-2005 |
| mCherry | Rockland | Cat# 600-401-P16 |
| Goat anti-rabbit AlexaFluor 594 secondary | ThermoFisher | Cat# A-11012 |
| **Bacterial and Virus Strains** | | |
| West Nile Virus Texas 2002-HC | Gale Laboratory | N/A |
| **Chemicals, Peptides, and Recombinant Proteins** | | |
| *all-trans* retinoic acid | Sigma-Aldrich | Cat# R2625 |
| Human BDNF | Peprotech | Cat# 450-02 |
| Murine M-CSF | Peprotech | Cat# 315-02 |
| Sytox Green | ThermoFisher | Cat# S7020 |
| Syto Green 24 | ThermoFisher | Cat# S7599 |
| Collagenase A | Sigma-Aldrich | Cat# 11088793001 |
| DNAse I | Sigma-Aldrich | Cat# D4263 |
| Percoll | Sigma-Aldrich | Cat# P1644 |
| Poly(I:C) | Millipore | Cat# 528906 |
| LPS-EB Ultrapure | Invivogen | Cat# Tlrl-3pelps |
| CL264 | Invivogen | Cat# Tlrl-c264e |
| zVAD | SM Biochemicals | Cat# SMFMK001 |
| Necrostatin-1 | Sigma-Aldrich | Cat# N9037 |
| GSK 843 | GlaxoSmithKline | N/A |
| GSK 872 | GlaxoSmithKline | N/A |
| GSK 963 | GlaxoSmithKline | N/A |

| REAGENT or RESOURCE | SOURCE | IDENTIFIER |
|---|---|---|
| QVD | SM Biochemicals | Cat# SMPH001 |
| AP1 (BB Homodimerizer) | Clontech | Cat# 635069 |
| Murine TNF-α | Peprotech | Cat# 315-01A |
| Cycloheximide | Sigma-Aldrich | Cat# C7698 |
| DAPI | ThermoFisher | Cat# 62248 |
| **Critical Commercial Assays** | | |
| Viral RNA Mini Kit | Qiagen | Cat# 52904 |
| NucleoSpin RNA Kit | Macherey-Nagel | Cat# 740955 |
| Human CCL2 ELISA Kit | Affymetrix | Cat# 88-7399-22 |
| Murine CCL2 ELISA Kit | Affymetrix | Cat# 88-7391-76 |
| Bio-Plex Pro Mouse Cytokine 23-plex Assay | Bio-Rad | Cat# M60009RDPD |
| **Experimental Models: Cell Lines** | | |
| BHK-21 | ATCC | Cat# CCL-10 |
| **Experimental Models: Organisms/Strains** | | |
| C57BL/6J | Jackson Laboratory | Stock# 000664 |
| C57BL/6NJ | Jackson Laboratory | Stock# 005304 |
| *Ripk3*$^{-/-}$ | Oberst Laboratory | N/A |
| *Mlkl*$^{-/-}$ | Oberst Laboratory | N/A |
| *Mlkl*$^{-/-}$ *Casp8*$^{-/-}$ | Oberst Laboratory | N/A |
| Mox2-Cre$^{+}$ | Jackson Laboratory | Stock# 003755 |
| RIPK3-2xFV$^{fl/fl}$ | Oberst Laboratory | N/A |
| *Ripk1*$^{KD/KD}$ | GlaxoSmithKline | N/A |
| **Oligonucleotides** | | |
| See Table S1 | | |
| **Software and Algorithms** | | |
| Prism version 7 | GraphPad Software | graphpad.com |
| FlowJo version 10 | FlowJo, LLC | flowjo.com |

## Supplementary Material

Refer to Web version on PubMed Central for supplementary material.

## Acknowledgments

We thank Megan L. Knoll for technical assistance. We thank Piper Treuting and the UW Histology and Imaging Core for assistance with histological preparations. We also thank John Bertin and the PRR DPU of GlaxoSmithKline for generously providing RIPK1 and RIPK3 inhibitors and *Ripk1*$^{KD/KD}$ mice used in this study. This was work was supported by NIH grants R01 AI108685 and R21 NS101524 (to AO), U19 AI083019 (to MG), and the NIH Intramural Research Program 1ZIAES10328601 (to JM). AGS was supported by a National Science Foundation Graduate Research Fellowship (DGE-1256082).

## References


Bardina SV, Michlmayr D, Hoffman KW, Obara CJ, Sum J, Charo IF, Lu W, Pletnev AG, Lim JK. Differential Roles of Chemokines CCL2 and CCL7 in Monocytosis and Leukocyte Migration during West Nile Virus Infection. J Immunol. 2015; 195:4306–4318. [PubMed: 26401006]

Beisner DR, Ch'en IL, Kolla RV, Hoffmann A, Hedrick SM. Cutting edge: innate immunity conferred by B cells is regulated by caspase-8. J Immunol. 2005; 175:3469–3473. [PubMed: 16148088]

Berger SB, Harris P, Nagilla R, Kasparcova V, Hoffman S, Swift B, Dare L, Schaeffer M, Capriotti C, Ouellette M, et al. Characterization of GSK'963: a structurally distinct, potent and selective inhibitor of RIP1 kinase. Cell Death Discov. 2015; 1:15009. [PubMed: 27551444]

Berger SB, Kasparcova V, Hoffman S, Swift B, Dare L, Schaeffer M, Capriotti C, Cook M, Finger J, Hughes-Earle A, et al. Cutting Edge: RIP1 kinase activity is dispensable for normal development but is a key regulator of inflammation in SHARPIN-deficient mice. J Immunol. 2014; 192:5476–5480. [PubMed: 24821972]

Brien JD, Lazear HM, Diamond MS. Propagation, quantification, detection, and storage of West Nile virus. Current protocols in microbiology. 2013; 31:15D 13 11–15D 13 18.

Cameron JS, Alexopoulou L, Sloane JA, DiBernardo AB, Ma Y, Kosaras B, Flavell R, Strittmatter SM, Volpe J, Sidman R, et al. Toll-like receptor 3 is a potent negative regulator of axonal growth in mammals. J Neurosci. 2007; 27:13033–13041. [PubMed: 18032677]

Cho H, Diamond MS. Immune responses to West Nile virus infection in the central nervous system. Viruses. 2012; 4:3812–3830. [PubMed: 23247502]

Cho YS, Challa S, Moquin D, Genga R, Ray TD, Guildford M, Chan FK. Phosphorylation-driven assembly of the RIP1-RIP3 complex regulates programmed necrosis and virus-induced inflammation. Cell. 2009; 137:1112–1123. [PubMed: 19524513]

Daniels BP, Holman DW, Cruz-Orengo L, Jujjavarapu H, Durrant DM, Klein RS. Viral pathogen-associated molecular patterns regulate blood-brain barrier integrity via competing innate cytokine signals. MBio. 2014; 5:e01476–01414. [PubMed: 25161189]

Daniels BP, Jujjavarapu H, Durrant DM, Williams JL, Green RR, White JP, Lazear HM, Gale M Jr, Diamond MS, Klein RS. Regional astrocyte IFN signaling restricts pathogenesis during neurotropic viral infection. J Clin Invest. 2017

Daniels BP, Klein RS. Viral sensing at the blood-brain barrier: new roles for innate immunity at the CNS vasculature. Clin Pharmacol Ther. 2015; 97:372–379. [PubMed: 25670037]

Degterev A, Hitomi J, Germscheid M, Ch'en IL, Korkina O, Teng X, Abbott D, Cuny GD, Yuan C, Wagner G, et al. Identification of RIP1 kinase as a specific cellular target of necrostatins. Nature chemical biology. 2008; 4:313–321. [PubMed: 18408713]

Diamond MS, Sitati EM, Friend LD, Higgs S, Shrestha B, Engle M. A critical role for induced IgM in the protection against West Nile virus infection. J Exp Med. 2003; 198:1853–1862. [PubMed: 14662909]

Durrant DM, Daniels BP, Klein RS. IL-1R1 signaling regulates CXCL12-mediated T cell localization and fate within the central nervous system during West Nile Virus encephalitis. J Immunol. 2014a; 193:4095–4106. [PubMed: 25200953]

Durrant DM, Daniels BP, Pasieka T, Dorsey D, Klein RS. CCR5 limits cortical viral loads during West Nile virus infection of the central nervous system. J Neuroinflammation. 2015; 12:233. [PubMed: 26667390]

Durrant DM, Robinette ML, Klein RS. IL-1R1 is required for dendritic cell-mediated T cell reactivation within the CNS during West Nile virus encephalitis. J Exp Med. 2013; 210:503–516. [PubMed: 23460727]

Durrant DM, Williams JL, Daniels BP, Klein RS. Chemokines Referee Inflammation within the Central Nervous System during Infection and Disease. Advances in medicine. 2014b; 2014:806741. [PubMed: 26556427]

Encinas M, Iglesias M, Liu Y, Wang H, Muhaisen A, Cena V, Gallego C, Comella JX. Sequential treatment of SH-SY5Y cells with retinoic acid and brain-derived neurotrophic factor gives rise to fully differentiated, neurotrophic factor-dependent, human neuron-like cells. J Neurochem. 2000; 75:991–1003. [PubMed: 10936180]

Getts DR, Terry RL, Getts MT, Muller M, Rana S, Shrestha B, Radford J, Van Rooijen N, Campbell IL, King NJ. Ly6c+ “inflammatory monocytes” are microglial precursors recruited in a pathogenic manner in West Nile virus encephalitis. J Exp Med. 2008; 205:2319–2337. [PubMed: 18779347]

Graham JB, Thomas S, Swarts J, McMillan AA, Ferris MT, Suthar MS, Treuting PM, Ireton R, Gale M Jr, Lund JM. Genetic diversity in the collaborative cross model recapitulates human West Nile virus disease outcomes. MBio. 2015; 6:e00493–00415. [PubMed: 25944860]

Gutierrez KD, Davis MA, Daniels BP, Olsen TM, Ralli-Jain P, Tait SW, Gale M Jr, Oberst A. MLKL Activation Triggers NLRP3-Mediated Processing and Release of IL-1beta Independently of Gasdermin-D. J Immunol. 2017; 198:2156–2164. [PubMed: 28130493]

He S, Liang Y, Shao F, Wang X. Toll-like receptors activate programmed necrosis in macrophages through a receptor-interacting kinase-3-mediated pathway. Proc Natl Acad Sci U S A. 2011; 108:20054–20059. [PubMed: 22123964]

Huang Z, Wu SQ, Liang Y, Zhou X, Chen W, Li L, Wu J, Zhuang Q, Chen C, Li J, et al. RIP1/RIP3 binding to HSV-1 ICP6 initiates necroptosis to restrict virus propagation in mice. Cell Host Microbe. 2015; 17:229–242. [PubMed: 25674982]

Ito Y, Ofengeim D, Najafov A, Das S, Saberi S, Li Y, Hitomi J, Zhu H, Chen H, Mayo L, et al. RIPK1 mediates axonal degeneration by promoting inflammation and necroptosis in ALS. Science. 2016; 353:603–608. [PubMed: 27493188]

Kaiser WJ, Sridharan H, Huang C, Mandal P, Upton JW, Gough PJ, Sehon CA, Marquis RW, Bertin J, Mocarski ES. Toll-like receptor 3-mediated necrosis via TRIF, RIP3, and MLKL. J Biol Chem. 2013; 288:31268–31279. [PubMed: 24019532]

Keller BC, Fredericksen BL, Samuel MA, Mock RE, Mason PW, Diamond MS, Gale M Jr. Resistance to alpha/beta interferon is a determinant of West Nile virus replication fitness and virulence. J Virol. 2006; 80:9424–9434. [PubMed: 16973548]

Klein RS, Lin E, Zhang B, Luster AD, Tollett J, Samuel MA, Engle M, Diamond MS. Neuronal CXCL10 directs CD8+ T-cell recruitment and control of West Nile virus encephalitis. J Virol. 2005; 79:11457–11466. [PubMed: 16103196]

Kok WM. New developments in flavivirus drug discovery. Expert opinion on drug discovery. 2016; 11:433–445. [PubMed: 26966889]

Kumar M, Roe K, Orillo B, Muruve DA, Nerurkar VR, Gale M Jr, Verma S. Inflammasome adaptor protein Apoptosis-associated speck-like protein containing CARD (ASC) is critical for the immune response and survival in west Nile virus encephalitis. J Virol. 2013; 87:3655–3667. [PubMed: 23302887]

Lawlor KE, Khan N, Mildenhall A, Gerlic M, Croker BA, D’Cruz AA, Hall C, Kaur Spall S, Anderton H, Masters SL, et al. RIPK3 promotes cell death and NLRP3 inflammasome activation in the absence of MLKL. Nat Commun. 2015; 6:6282. [PubMed: 25693118]

Lim JK, Obara CJ, Rivollier A, Pletnev AG, Kelsall BL, Murphy PM. Chemokine receptor Ccr2 is critical for monocyte accumulation and survival in West Nile virus encephalitis. J Immunol. 2011; 186:471–478. [PubMed: 21131425]

Liu T, Zhao DX, Cui H, Chen L, Bao YH, Wang Y, Jiang JY. Therapeutic hypothermia attenuates tissue damage and cytokine expression after traumatic brain injury by inhibiting necroptosis in the rat. Sci Rep. 2016; 6:24547. [PubMed: 27080932]

Mandal P, Berger SB, Pillay S, Moriwaki K, Huang C, Guo H, Lich JD, Finger J, Kasparcova V, Votta B, et al. RIP3 induces apoptosis independent of pronecrotic kinase activity. Molecular cell. 2014; 56:481–495. [PubMed: 25459880]

Michaelis M, Kleinschmidt MC, Doerr HW, Cinatl J Jr. Minocycline inhibits West Nile virus replication and apoptosis in human neuronal cells. The Journal of antimicrobial chemotherapy. 2007; 60:981–986. [PubMed: 17872917]

Moriwaki K, Bertin J, Gough PJ, Chan FK. A RIPK3-caspase 8 complex mediates atypical pro-IL-1beta processing. J Immunol. 2015; 194:1938–1944. [PubMed: 25567679]

Moriwaki K, Chan FK. Necroptosis-independent signaling by the RIP kinases in inflammation. Cellular and molecular life sciences: CMLS. 2016; 73:2325–2334. [PubMed: 27048814]

Murphy JM, Czabotar PE, Hildebrand JM, Lucet IS, Zhang JG, Alvarez-Diaz S, Lewis R, Lalaoui N, Metcalf D, Webb AI, et al. The pseudokinase MLKL mediates necroptosis via a molecular switch mechanism. Immunity. 2013; 39:443–453. [PubMed: 24012422]

Najjar M, Saleh D, Zelic M, Nogusa S, Shah S, Tai A, Finger JN, Polykratis A, Gough PJ, Bertin J, et al. RIPK1 and RIPK3 Kinases Promote Cell-Death-Independent Inflammation by Toll-like Receptor 4. Immunity. 2016; 45:46–59. [PubMed: 27396959]

Newton K, Dugger DL, Maltzman A, Greve JM, Hedehus M, Martin-McNulty B, Carano RA, Cao TC, van Bruggen N, Bernstein L, et al. RIPK3 deficiency or catalytically inactive RIPK1 provides greater benefit than MLKL deficiency in mouse models of inflammation and tissue injury. Cell death and differentiation. 2016

Newton K, Sun X, Dixit VM. Kinase RIP3 is dispensable for normal NF-kappa Bs, signaling by the B-cell and T-cell receptors, tumor necrosis factor receptor 1, and Toll-like receptors 2 and 4. Mol Cell Biol. 2004; 24:1464–1469. [PubMed: 14749364]

Nogusa S, Thapa RJ, Dillon CP, Liedmann S, Oguin TH 3rd, Ingram JP, Rodriguez DA, Kosoff R, Sharma S, Sturm O, et al. RIPK3 Activates Parallel Pathways of MLKL-Driven Necroptosis and FADD-Mediated Apoptosis to Protect against Influenza A Virus. Cell Host Microbe. 2016; 20:13–24. [PubMed: 27321907]

Oberst A. Death in the fast lane: what's next for necroptosis? The FEBS journal. 2015

Ofengeim D, Ito Y, Najafov A, Zhang Y, Shan B, DeWitt JP, Ye J, Zhang X, Chang A, Vakifahmetoglu-Norberg H, et al. Activation of necroptosis in multiple sclerosis. Cell reports. 2015; 10:1836–1849. [PubMed: 25801023]

Orozco S, Yatim N, Werner MR, Tran H, Gunja SY, Tait SW, Albert ML, Green DR, Oberst A. RIPK1 both positively and negatively regulates RIPK3 oligomerization and necroptosis. Cell death and differentiation. 2014; 21:1511–1521. [PubMed: 24902904]

Pan Q, Huang Y, Chen L, Gu J, Zhou X. SMAC-armed vaccinia virus induces both apoptosis and necroptosis and synergizes the efficiency of vinblastine in HCC. Human cell. 2014; 27:162–171. [PubMed: 24771354]

Ramos HJ, Lanteri MC, Blahnik G, Negash A, Suthar MS, Brassil MM, Sodhi K, Treuting PM, Busch MP, Norris PJ, et al. IL-1beta signaling promotes CNS-intrinsic immune control of West Nile virus infection. PLoS Pathog. 2012; 8:e1003039. [PubMed: 23209411]

Ransohoff RM, Trettel F. Editorial Research Topic "Chemokines and chemokine receptors in brain homeostasis". Front Cell Neurosci. 2015; 9:132. [PubMed: 25904848]

Re DB, Le Verche V, Yu C, Amoroso MW, Politi KA, Phani S, Ikiz B, Hoffmann L, Koolen M, Nagata T, et al. Necroptosis drives motor neuron death in models of both sporadic and familial ALS. Neuron. 2014; 81:1001–1008. [PubMed: 24508385]

Reaux-Le Goazigo A, Van Steenwinckel J, Rostene W, Melik Parsadaniantz S. Current status of chemokines in the adult CNS. Prog Neurobiol. 2013; 104:67–92. [PubMed: 23454481]

Samuel MA, Morrey JD, Diamond MS. Caspase 3-dependent cell death of neurons contributes to the pathogenesis of West Nile virus encephalitis. J Virol. 2007; 81:2614–2623. [PubMed: 17192305]

Samuel MA, Whitby K, Keller BC, Marri A, Barchet W, Williams BR, Silverman RH, Gale M Jr, Diamond MS. PKR and RNase L contribute to protection against lethal West Nile Virus infection by controlling early viral spread in the periphery and replication in neurons. J Virol. 2006; 80:7009–7019. [PubMed: 16809306]

Sejvar JJ, Haddad MB, Tierney BC, Campbell GL, Marfin AA, Van Gerpen JA, Fleischauer A, Leis AA, Stokic DS, Petersen LR. Neurologic manifestations and outcome of West Nile virus infection. JAMA. 2003; 290:511–515. [PubMed: 12876094]

Suthar MS, Diamond MS, Gale M Jr. West Nile virus infection and immunity. Nature reviews Microbiology. 2013; 11:115–128. [PubMed: 23321534]

Szretter KJ, Daniels BP, Cho H, Gainey MD, Yokoyama WM, Gale M Jr, Virgin HW, Klein RS, Sen GC, Diamond MS. 2′-O methylation of the viral mRNA cap by West Nile virus evades ifit1-dependent and -independent mechanisms of host restriction in vivo. PLoS Pathog. 2012; 8:e1002698. [PubMed: 22589727]

Takahashi N, Duprez L, Grootjans S, Cauwels A, Nerinckx W, DuHadaway JB, Goossens V, Roelandt R, Van Hauwermeiren F, Libert C, et al. Necrostatin-1 analogues: critical issues on the specificity,

activity and in vivo use in experimental disease models. Cell Death Dis. 2012; 3:e437. [PubMed: 23190609]

Teitz T, Wei T, Valentine MB, Vanin EF, Grenet J, Valentine VA, Behm FG, Look AT, Lahti JM, Kidd VJ. Caspase 8 is deleted or silenced preferentially in childhood neuroblastomas with amplification of MYCN. Nat Med. 2000; 6:529–535. [PubMed: 10802708]

Upton JW, Kaiser WJ, Mocarski ES. Virus inhibition of RIP3-dependent necrosis. Cell Host Microbe. 2010; 7:302–313. [PubMed: 20413098]

Upton JW, Kaiser WJ, Mocarski ES. DAI/ZBP1/DLM-1 complexes with RIP3 to mediate virus-induced programmed necrosis that is targeted by murine cytomegalovirus vIRA. Cell Host Microbe. 2012; 11:290–297. [PubMed: 22423968]

Vasek MJ, Garber C, Dorsey D, Durrant DM, Bollman B, Soung A, Yu J, Perez-Torres C, Frouin A, Wilton DK, et al. A complement-microglial axis drives synapse loss during virus-induced memory impairment. Nature. 2016; 534:538–543. [PubMed: 27337340]

Vitner EB, Salomon R, Farfel-Becker T, Meshcheriakova A, Ali M, Klein AD, Platt FM, Cox TM, Futerman AH. RIPK3 as a potential therapeutic target for Gaucher's disease. Nat Med. 2014; 20:204–208. [PubMed: 24441827]

Wang H, Sun L, Su L, Rizo J, Liu L, Wang LF, Wang FS, Wang X. Mixed lineage kinase domain-like protein MLKL causes necrotic membrane disruption upon phosphorylation by RIP3. Molecular cell. 2014a; 54:133–146. [PubMed: 24703947]

Wang X, Jiang W, Yan Y, Gong T, Han J, Tian Z, Zhou R. RNA viruses promote activation of the NLRP3 inflammasome through a RIP1-RIP3-DRP1 signaling pathway. Nat Immunol. 2014b; 15:1126–1133. [PubMed: 25326752]

Wang Y, Lobigs M, Lee E, Mullbacher A. CD8+ T cells mediate recovery and immunopathology in West Nile virus encephalitis. J Virol. 2003; 77:13323–13334. [PubMed: 14645588]

Williams JL, Holman DW, Klein RS. Chemokines in the balance: maintenance of homeostasis and protection at CNS barriers. Front Cell Neurosci. 2014a; 8:154. [PubMed: 24920943]

Williams JL, Patel JR, Daniels BP, Klein RS. Targeting CXCR7/ACKR3 as a therapeutic strategy to promote remyelination in the adult central nervous system. J Exp Med. 2014b; 211:791–799. [PubMed: 24733828]

Xu Y, Wang J, Song X, Qu L, Wei R, He F, Wang K, Luo B. RIP3 induces ischemic neuronal DNA degradation and programmed necrosis in rat via AIF. Sci Rep. 2016; 6:29362. [PubMed: 27377128]

Yatim N, Jusforgues-Saklani H, Orozco S, Schulz O, Barreira da Silva R, Reis e Sousa C, Green DR, Oberst A, Albert ML. RIPK1 and NF-kappaB signaling in dying cells determines cross-priming of CD8(+) T cells. Science. 2015; 350:328–334. [PubMed: 26405229]

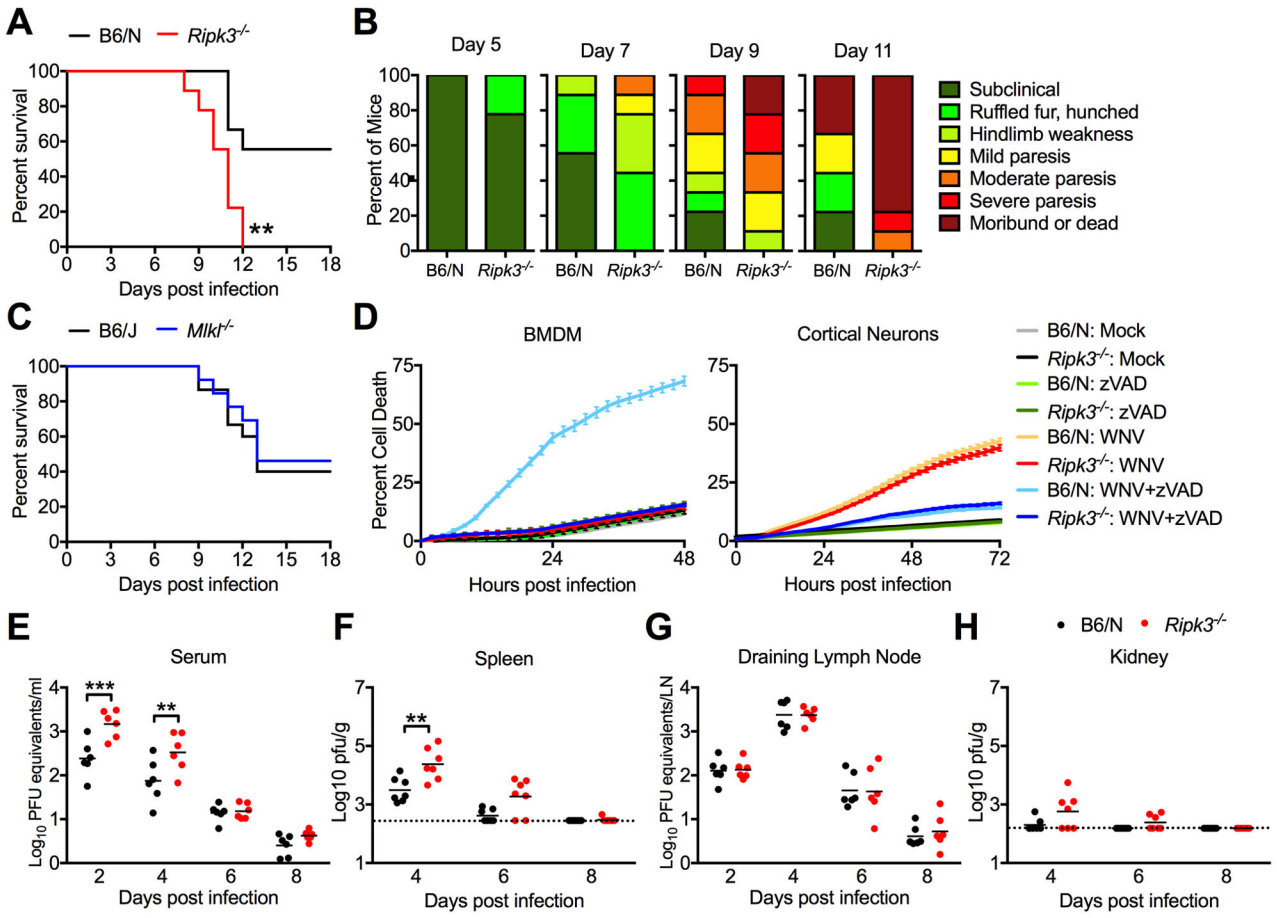


**Figure 1. RIPK3 limits WNV pathogenesis independently of MLKL and cell death**

(A) Survival analysis in 8 week old *Ripk3*$^{-/-}$ mice and age/sex matched congenic C57BL/6NJ controls (B6/N) following subcutaneous inoculation with 100pfu WNV-TX. N= 9 mice/genotype.

(B) Presentation of clinical signs of disease in B6/N or *Ripk3*$^{-/-}$ mice on indicated days following subcutaneous WNV infection. N= 9 mice/genotype.

(C) Survival analysis in 8 week old *Mlkl*$^{-/-}$ mice and age/sex matched congenic C57BL/6J controls (B6/J) following subcutaneous inoculation with 100pfu WNV-TX. N= 15(B6/J) or 13 (*Mlkl*$^{-/-}$).

(D) Kinetics of cell death in primary bone-marrow derived macrophage (BMDM) or cortical neuron (CN) cultures after infection with 0.01 (BMDM) or 0.001 (CN) MOI WNV-TX, with or without co-treatment with the pan-caspase inhibitor zVAD. Cell death was determined by Sytox Green uptake and quantified as the percent of total cell nuclei that are Sytox Green-positive. N= 3 (BMDM) or 6 (CN).

(E–H) 8 week old B6/N or *Ripk3*$^{-/-}$ mice were infected subcutaneously with 100 pfu WNV-TX. On indicated days following infection, the indicated tissues were harvested, weighed, homogenized, and assayed for WNV titers via qRT-PCR (E,G) or plaque assay (F,H). qRT-PCR data are normalized against a standard curve of known viral titers to generate plaque-forming unit (pfu) equivalents (E,G).

-**p<0.01, ***p<0.001. Error bars represent SEM. Dotted lines indicate limits of detection. All data are pooled from two or three independent experiments.
See also related figures S1 and S2.

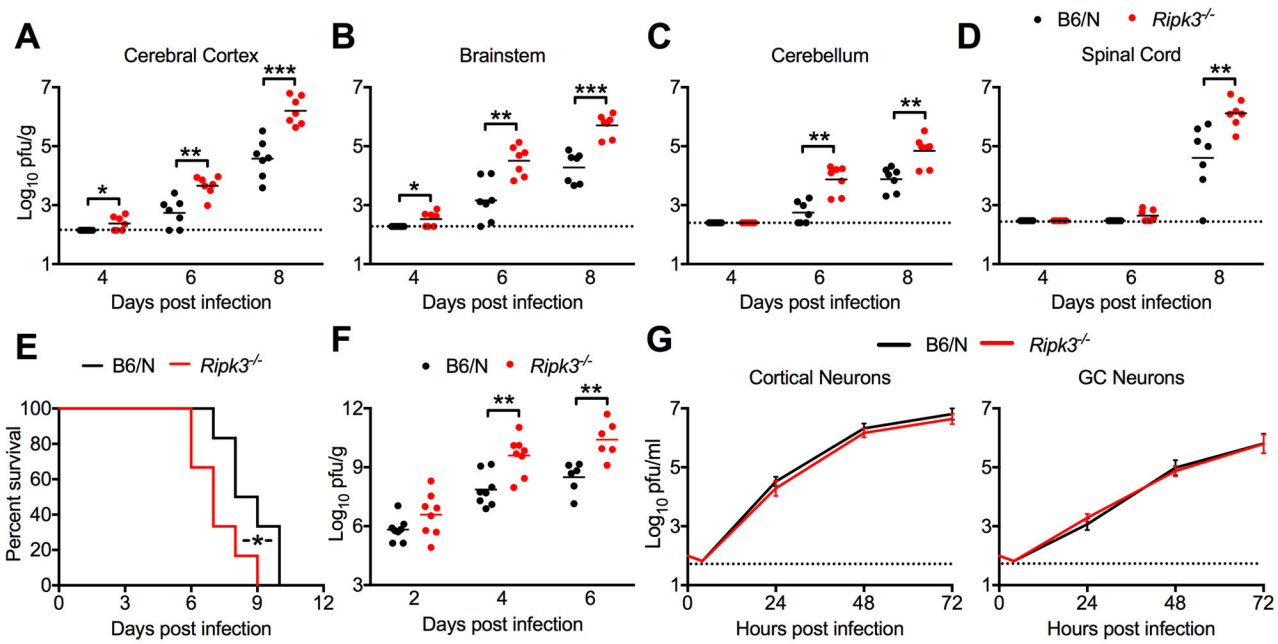


**Figure 2. RIPK3 restricts WNV replication in the CNS in a neuron-extrinsic manner**

(A–D) 8 week old B6/N or *Ripk3*$^{-/-}$ mice were infected subcutaneously with 100 pfu WNV-TX. On indicated days following infection, the indicated tissues were harvested, weighed, homogenized, and WNV titers measured via plaque assay.

(E) Survival analysis in 8 week old *Ripk3*$^{-/-}$ mice and age/sex matched congenic C57BL/6NJ controls (B6/N) following intracranial inoculation with 10pfu WNV-TX. N=6 mice/genotype.

(F) 8 week old B6/N or *Ripk3*$^{-/-}$ mice were infected intracranially with 10 pfu WNV-TX. On indicated days following infection, whole brains were harvested, weighed, homogenized, and WNV titers were measured via plaque assay.

(G) Multistep viral growth curve analysis in primary B6/N or *Ripk3*$^{-/-}$ cortical neuron or cerebellar granule cell neuron cultures following infection with 0.001 MOI WNV-TX. N= 9 (C) or 6 (D).

-*p<0.05, **p<0.01, ***p<0.001. Dotted lines indicate limits of detection. All data are pooled from two or three independent experiments.

See also related figure S3.

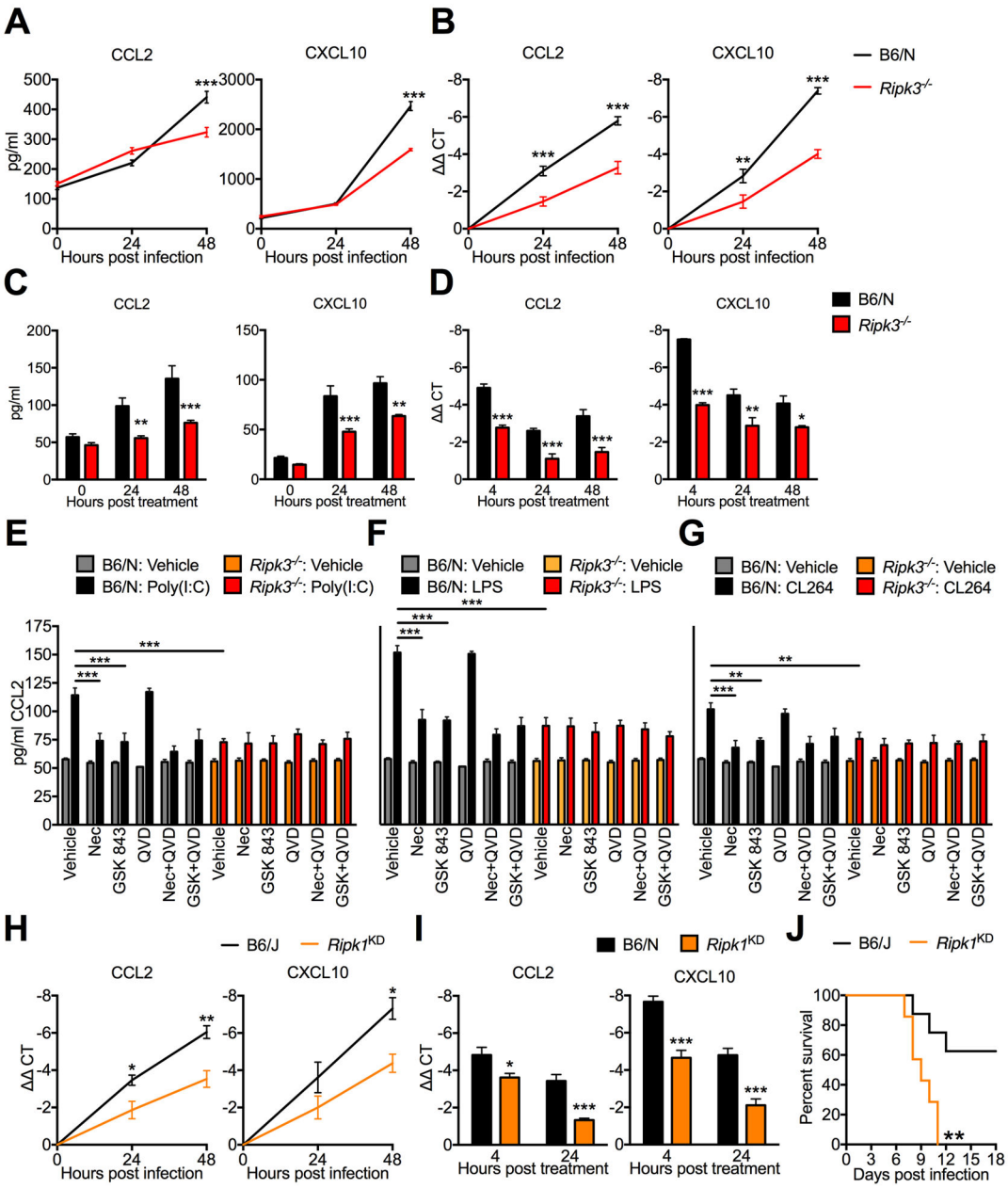


**Figure 3. RIPK3-mediated neuronal chemokine expression occurs downstream of multiple TLRs and requires the kinase activity of RIPK1 and RIPK3**

(A–D) CCL2 or CXCL10 expression in B6/N or *Ripk3*$^{-/-}$ cortical neuron cultures following infection with 0.001 MOI WNV-TX (A–B) or treatment with 1 μg/ml poly(I:C) (C–D), measuring protein in supernatant via Bio-plex multiplex immunoassay assay (A,C) or mRNA expression in cells via qRT-PCR (B,D). N=3–6 replicates/group.

(E–G) CCL2 expression measured by ELISA in cortical neuron culture supernatants after 24h treatment with 1 μg/ml poly(I:C) (E), 1 μg/ml LPS (F), or 1 μg/ml CL264 (G). Prior to addition of TLR agonist, cells were pretreated for 1h with 30 μM Necrostatin-1 (Nec), 100 nM GSK 843, and/or 2 μM QVD. Inhibitors remained in culture medium for the duration of the experiment. As experiments in (C–E) happened concurrently, data with each TLR

agonist is compared against a single set of vehicle controls (gray and orange bars), the data for which is repeated in each panel. N=4 replicates/group.

(H–I) CCL2 or CXCL10 expression in B6/J or *Ripk1*$^{KD/KD}$ cortical neuron cultures following infection with 0.001 MOI WNV-TX (H) or treatment with 1 μg/ml poly(I:C) (I), measured via qRT-PCR. N=4 replicates/group.

(J) Survival analysis in 8 week old *Ripk1*$^{KD/KD}$ mice and B6/J controls following subcutaneous inoculation with 100pfu WNV-TX. N=7 mice/genotype.

-*p<0.05, **p<0.01, ***p<0.001. Error bars represent SEM. All data are pooled from at least two independent experiments.

See also related figures S4 and S5.

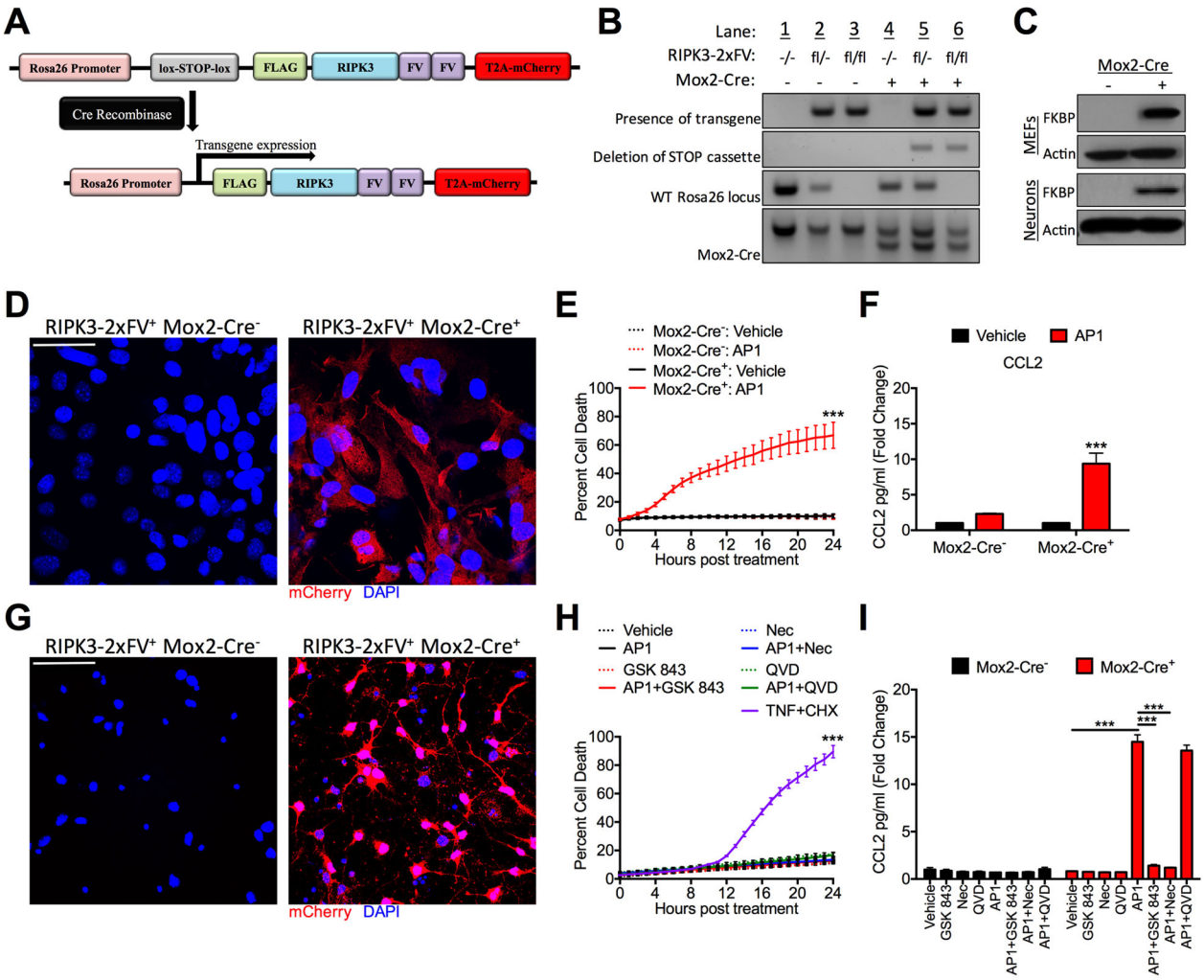


**Figure 4. RIPK3 activation alone is sufficient to drive neuronal chemokine expression**

A) Schematic illustrating the transgene construct and Cre-mediated deletion of the stop cassette driving transgene expression.

(B) DNA gels depicting genotyping strategy for RIPK3-2xFV$^{fl/fl}$ Mox2-Cre$^{+}$ mice. Top row: presence of RIPK3-2xFV transgene; second row: RIPK3-2xFV transgene with deleted stop cassette; third row: confirmation of transgene homozygosity by detecting absence of WT *Rosa*26 locus; fourth row: detection of Mox2-Cre expression (smaller bp product). See methods.

(C) Western blot confirmation of FKBP expression in murine embryonic fibroblast (MEF) and cortical neuron cultures. Actin is included as a housekeeping control.

(D,G) Immunocytochemical detection of mCherry (red) and DAPI (blue) in primary murine embryonic fibroblast (MEF) (D) or cortical neuron cultures (G) of the indicated genotype. Images are representative of 3 replicates/genotype. Scale bar= 20μm (D) or 40μm (G).

(E, H) Kinetics of cell death in primary RIPK3-2xFV$^{fl/fl}$ Mox2-Cre$^{+}$ primary MEF (E) or cortical neuron cultures (H) after treatment with 100nM AP1 in the presence of indicated inhibitors. Combined treatment with TNF-α and cycloheximide served as a positive control

for cell death (H). Cell death was determined by Sytox Green uptake and quantified as the percent of total cell nuclei that are Sytox Green-positive. N= 2–4 replicates/group.
(F, I) CCL2 expression measured by ELISA in supernatants of RIPK3-2xFV$^{fl/fl}$ MEF (F) or cortical neuron (I) cultures of indicated genotype 24h after treatment with AP1 and/or indicated inhibitors. N= 3 replicates/group.
***p<0.001. Error bars represent SEM. All data are pooled from at least two independent experiments.

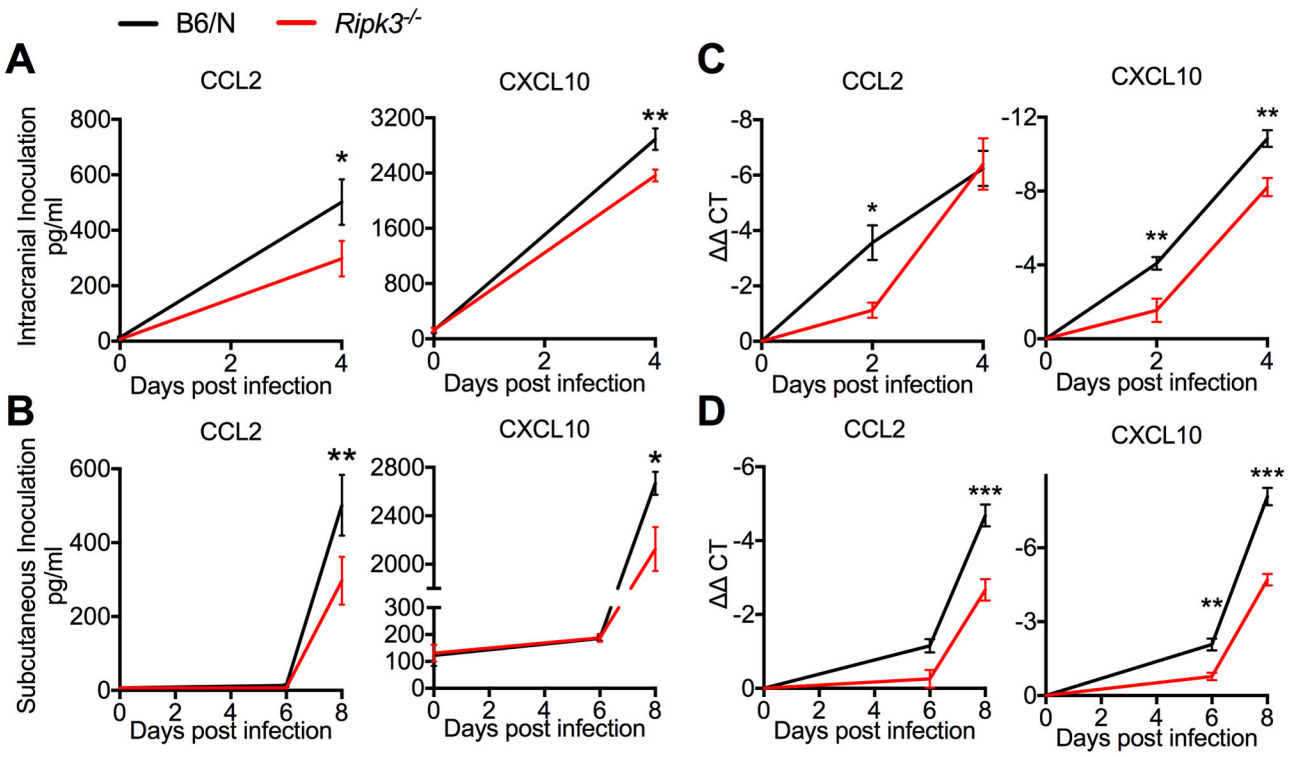


**Figure 5. RIPK3 enhances CNS chemokine expression after WNV infection**

(A–B) CCL2 (left) or CXCL10 (right) protein expression as determined by Bio-plex protein immunoassay in clarified brain homogenates taken on indicated days after either intracranial (A) or subcutaneous (B) WNV infection.

(C–D) CCL2 (left) or CXCL10 (right) mRNA expression as determined by qRT-PCR using RNA extracted from whole brains taken on indicated days after either intracranial (C) or subcutaneous

(D) WNV infection. Data are expressed as ΔΔCT, wherein CT values for individual samples are first normalized to the housekeeping gene *Gapdh,* then normalized against values for uninfected controls.

-*p<0.05, **p<0.01, ***p<0.001. Error bars represent SEM. N=6 for all panels. Data are pooled from two independent experiments.

See also related figure S6.

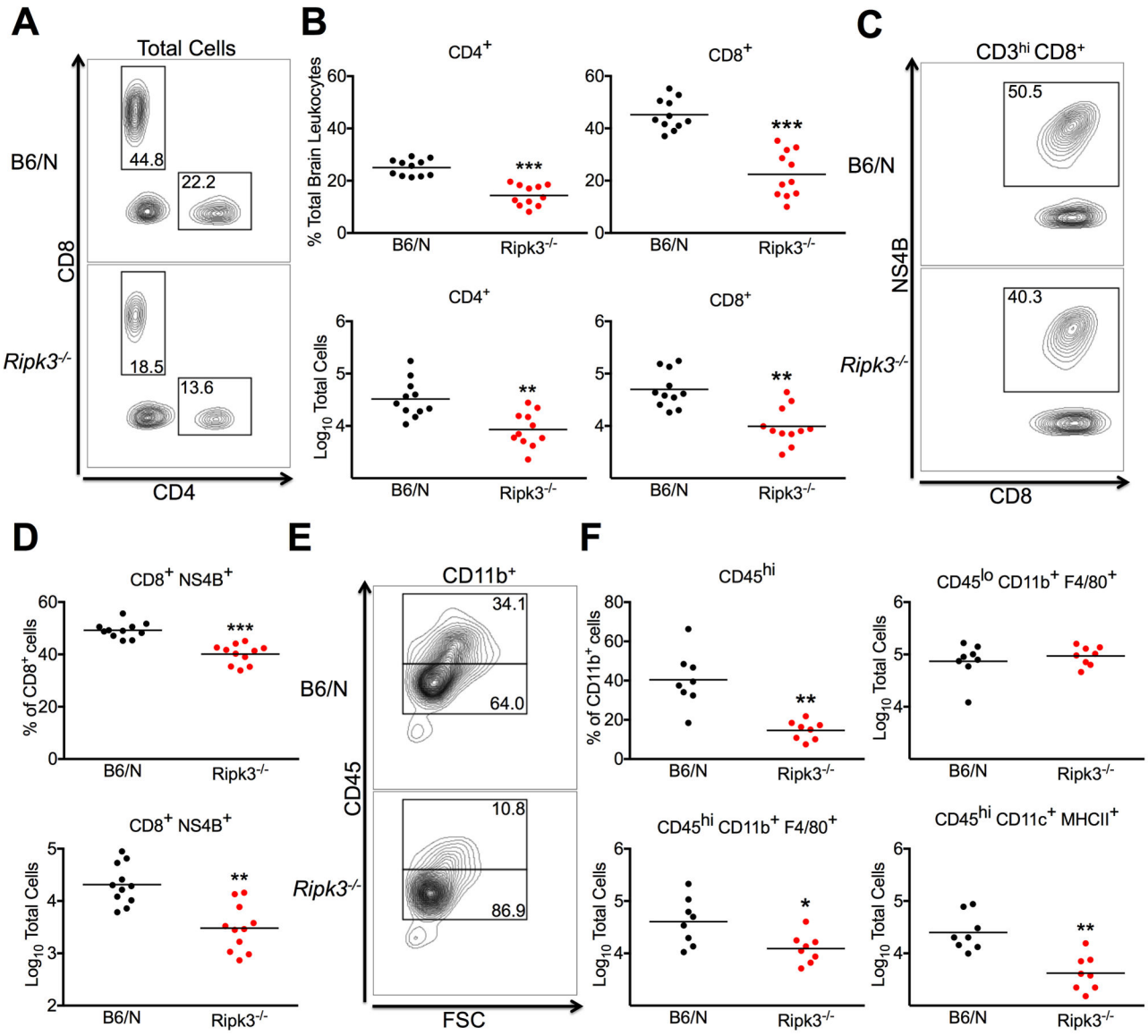


**Figure 6. RIPK3 coordinates CNS immune cell infiltration after WNV infection**

(A–F) Total brain leukocytes were isolated from B6/N or *Ripk3*$^{-/-}$ mice on day 8 following subcutaneous inoculation with WNV-TX.

(A) Representative flow cytometric plots showing CD4$^{+}$ and CD8$^{+}$ T cells among total brain leukocytes. Numbers represent percentage of cells in each gate relative to total plotted cells.

(B) Percentage (top row) and numbers (bottom row) of CD4$^{+}$ and CD8$^{+}$ T cells among total brain leukocytes.

(C) Representative plots showing cells stained with a tetramer displaying the immunodominant WNV peptide D$^{b}$-NS4B (NS4B) after prior gating for CD3$^{hi}$ and CD8$^{+}$ cells.

(D) Percentage of NS4B tetramer$^{+}$ cells among total CD8$^{+}$ T cells (top) or total number of CD8$^{+}$ NS4B$^{+}$ T cells collected from total brain leukocytes (bottom).

(E) Representative plots showing $CD45^{lo}$ vs. $CD45^{hi}$ expressing cells after prior gating for $CD11b^{+}$ cells.

(F) Percentage of $CD45^{hi}$ cells among total $CD11b^{+}$ cells (top left) or total numbers of cells expressing indicated markers collected from total brain leukocytes (top right and bottom row).

-*p<0.05, **p<0.01, ***p<0.001. Data are pooled from two or three independent experiments.

See also related figure S7.

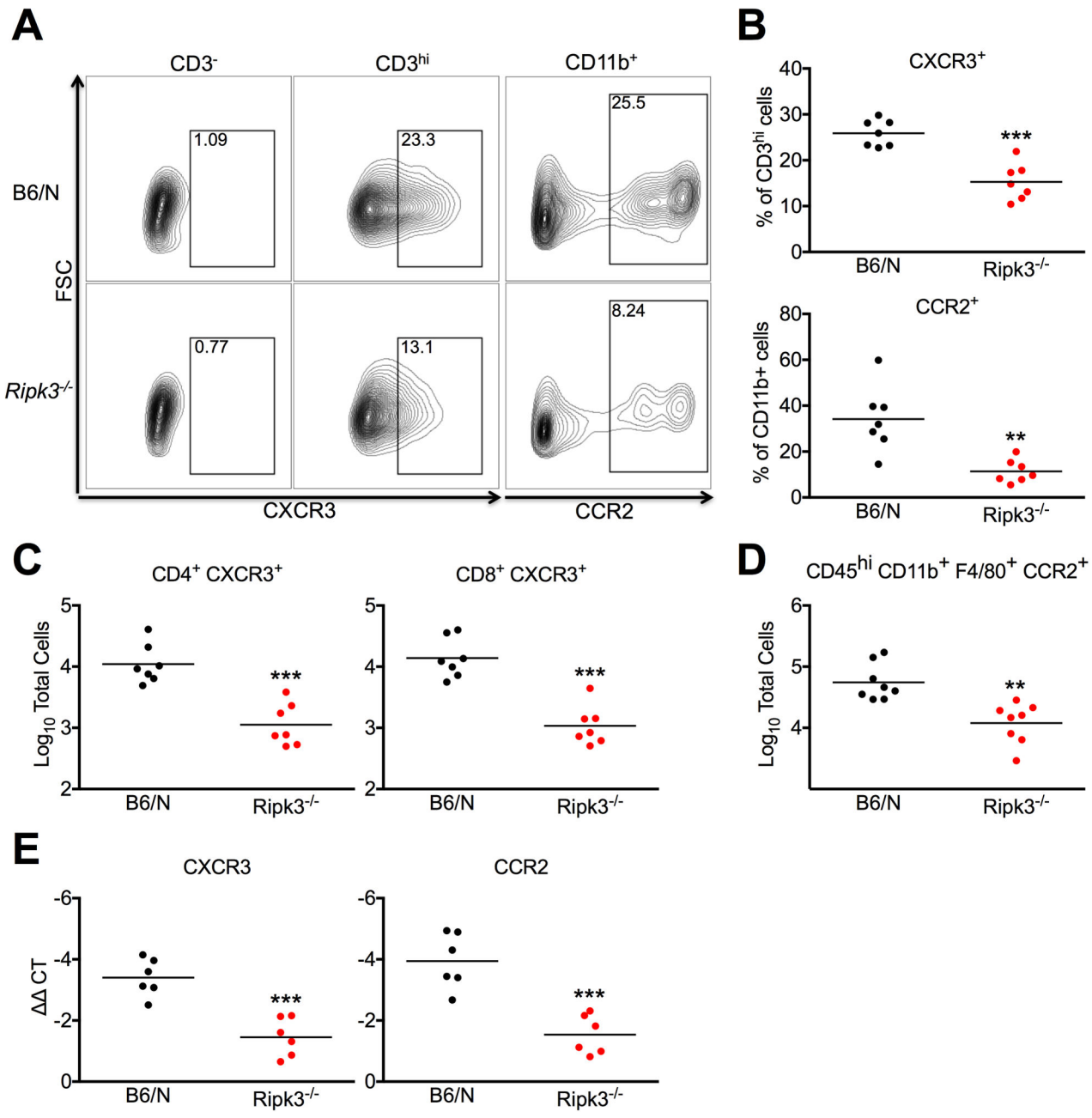


**Figure 7. RIPK3 mediates CNS recruitment of CXCR3$^+$ and CCR2$^+$ infiltrating leukocytes**

(A–F) Total brain leukocytes were isolated from B6/N or *Ripk3*$^{-/-}$ mice on day 8 following subcutaneous inoculation with WNV-TX.

(A) Representative flow cytometric plots showing CXCR3$^+$ cells after prior gating for CD3$^-$ or CD3$^+$ cells (left) or CCR2$^+$ cells after prior gating for CD11b$^+$ cells. Numbers represent percentage of cells in each gate relative to total plotted cells.

(B) Percentages of CXCR3$^+$ cells among total CD3$^{hi}$ cells (top) or CCR2$^+$ cells among total CD11b$^+$ cells (bottom).

(C–D) Total numbers of cells expressing indicated markers collected from total brain leukocytes.

(E) qRT-PCR analysis of CXCR3 or CCR2 expression using RNA extracted from whole brains on day 8 following subcutaneous WNV infection.

-**p<0.01, ***p<0.001. All data are pooled from two independent experiments.